Energy-Efficient Soft Error-Tolerant Digital Signal Processing

Byonghyo Shim, *Member, IEEE*, and Naresh R. Shanbhag, *Fellow, IEEE*

***Abstract*—In this paper, we present energy-efficient soft error-tolerant techniques for digital signal processing (DSP) systems. The proposed technique, referred to as algorithmic soft error-tolerance (ASET), employs low-complexity estimators of a main DSP block to achieve reliable operation in the presence of soft errors. Three distinct ASET techniques—spatial, temporal and spatio-temporal—are presented. For frequency selective finite-impulse response (FIR) filtering, it is shown that the proposed techniques provide robustness in the presence of soft error rates of up to $P_{\rm er} = 10^{-2}$ and $P_{\rm er} = 10^{-3}$ in a single-event upset scenario. The power dissipation of the proposed techniques ranges from 1.1 X to 1.7 X (spatial ASET) and 1.05 X to 1.17 X (spatio-temporal and temporal ASET) when the desired signal-to-noise ratio $\rm SNR_{des} = 25$ dB. In comparison, the power dissipation of the commonly employed triple modular redundancy technique is 2.9 X.**

***Index Terms*—Digital signal processing (DSP), low-power, reduced precision redundancy (RPR), reliability, soft error tolerance, triple modular redundancy (TMR).**

I. Introduction

REDUCED feature sizes and voltages in modern semiconductor process technologies have made current and future systems vulnerable to deep-submicron (DSM) noise [1], [3] and soft errors due to particle hits [4]–[17]. Particle hits result in voltage glitches at circuit nodes, which then may get captured by a latching element or flip a logic state.

Soft errors in semiconductor memories have been a known concern for many years. Error-correcting codes (ECCs) have been employed to combat soft errors in memories. Soft errors in logic and data-path circuits were not a problem in the past because particle hit-induced voltage glitches were masked [14] through the following three mechanisms: 1) attenuation of noise pulses as it propagates through a logic chain (electrical masking); 2) logic values overriding the noisy input (logical masking); and 3) noise pulse missing the latch setup and hold timing window (latching-window masking).

However, these masking mechanisms become less effective with reduction in feature size, increase in clock frequency, and reduction in pipelining depth of modern architectures. It has been shown that the critical charge which flips the internal state of a logic gate approaches 4fC in 0.13-μm technology [13], whereas, the generated charge due to a neutron particle hit can be up to 100fC [6]. In fact, it is reported that the soft error rate in logic circuits is expected to increase nine orders of magnitude from 1992 to 2011 to the point where soft error rates in logic will equal that of unprotected memory structures [14]. For these reasons, the 2003 International Technology Roadmap for Semiconductors (ITRS) [15] refers to error tolerance as a "cross cutting" challenge for the next decade. Soft-error tolerance is an important problem that needs to be addressed at the circuit, architectural, and algorithmic levels. In all cases, enhancing the robustness of systems and circuits to soft errors introduces redundancy in some form. Doing so results in an area and power overhead. Therefore, there is a fundamental tradeoff between energy efficiency and robustness [8].

In this paper, we extend our past work on algorithmic noise-tolerance (ANT) [23]–[26] for combating DSM noise. An ANT-based system is composed of an error-control (**EC**) block that detects and corrects errors in the main (**M**) block. A key underlying assumption in our past work was that the **EC** block is error-free. The rationale for this assumption is the fact that **EC** blocks are much smaller than the main block and, hence, can be designed to be robust to DSM noise source as voltage/frequency scaling, process variation, ground bounce, etc. Since this assumption is no longer valid in presence of particle hits, we relax this assumption in this paper.

The primary contributions of this paper are twofold.

1) We propose algorithmic soft-error tolerance (ASET) as a low-power technique for improving the robustness of DSP systems to soft errors. Three distinct ASET techniques are proposed: spatial, spatio-temporal, and temporal. We show that the energy overhead due to ASET is a factor of at least 3X smaller than that of the commonly employed triple modular redundancy (TMR) technique.
2) We analyze the algorithmic performance of the proposed ASET techniques. Specifically, we present a residual mean square error (rMSE) analysis which can be employed in the design of ASET-based DSP systems.

The rest of this paper is organized as follows. We introduce the soft error model and review past work in Section II. In Section III, we present the proposed ASET techniques. Section IV presents the analysis of ASET techniques. Simulation results and discussions are provided in Section V.

II. Soft Errors

In this section, we first discuss the soft error model which will be employed to study the effectiveness of the proposed ASET

Manuscript received January 17, 2005; revised September 28, 2005. This work was supported in part by the Microelectronics Advanced Research Corporation (MARCO) sponsored by the Gigascale System Research Center and in part by the National Science Foundation under Grant CCR 99-79381 and Grant CCR 00-85929.

B. Shim was with the University of Illinois at Urbana-Champaign, Urbana, IL 61801 USA. He is now with Qualcomm Inc., San Diego, CA 92121 USA (e-mail: bshim@qualcomm.com).

N. R. Shanbhag is with the Coordinated Science Laboratory, Department of Electrical and Computer Engineering, University of Illinois at Urbana-Champaign, Urbana, IL 61801 USA (e-mail: shanbhag@mail.icims.csl.uiuc.edu).

Digital Object Identifier 10.1109/TVLSI.2006.874359

techniques, and then review the past work on reliable computation. In this paper, we restrict our attention to the single event upset (SEU) model [5], which is commonly employed to study the effectiveness of soft error-tolerant systems.

A. Soft Error Model

Soft errors are caused by particle strikes such as high-energy neutrons or alpha particles. An expression for estimating the soft error rate (SER) $P_{\rm er}$ [5] is given by

$$P_{\rm er} = \frac{N}{T} \propto A \times F \times \exp\left(-\frac{Q_{\rm crit}}{Q_s}\right) \tag{1}$$

where A is the area, F is the particle flux, T is the observation period, $Q_{\rm crit}$ is the critical charge required to flip the logic value at a node, and Q_s is the collection efficiency. Typical SER for SRAM circuits for 0.13 μm is reported to be 100 kFIT/Mbit [16], where failure in time (FIT) is defined as the number of errors per one billion hours. As the technology scales, $Q_{\rm crit}$ reduces proportionally and so does Q_s. Hence, the probability of an effective particle hit at a node remains approximately the same. However, the number of nodes per chip increases while the clock period and pipeline depth reduces. Thus, chip-level soft error rate will increase [14].

In the presence of soft errors, the output $y_a[n]$ of a DSP system can be written as

$$y_a[n] = y_o[n] + \gamma[n] = \big(d[n] + \eta[n]\big) + \gamma[n] \tag{2}$$

where $y_o[n]$ denotes the error-free output composed of a desired signal $d[n]$ and noise $\eta[n]$, and $\gamma[n]$ is the soft error signal.

Assuming a $N+1$-bit 2's complement number representation, $y_o[n]$ can be represented as

$$y_o[n] = -b_0[n] + \sum_{i=1}^{N} b_i[n]2^{-i} \tag{3}$$

where $b_i[n]$ is the ith bit in a 2's complement representation of $y_o[n]$. We define a *flip variable* $f_i[n]$, where $f_i[n]=1$ indicates that the ith bit of $y_o[n]$ is flipped and $f_i[n]=0$ indicates otherwise. The rationale for employing the flip variable $f_i[n]$ is that the soft error occurs only when the voltage glitch generated by a particle hit propagates to an output and is captured by a latch (see Fig. 1).

If the flip vector $\boldsymbol{f}[n] = (f_0[n], f_1[n], \ldots, f_N[n])$ at time unit n is given, then the actual output $y_a[n]$ is expressed as

$$\begin{aligned} y_a[n] &= \boldsymbol{f}[n] \oplus y_o[n] \\ &= -\big(b_0[n] \oplus f_0[n]\big) + \sum_{i=1}^{N} \big(b_i[n] \oplus f_i[n]\big)2^{-i} \end{aligned} \tag{4}$$

where $\oplus$ is the XOR operation.

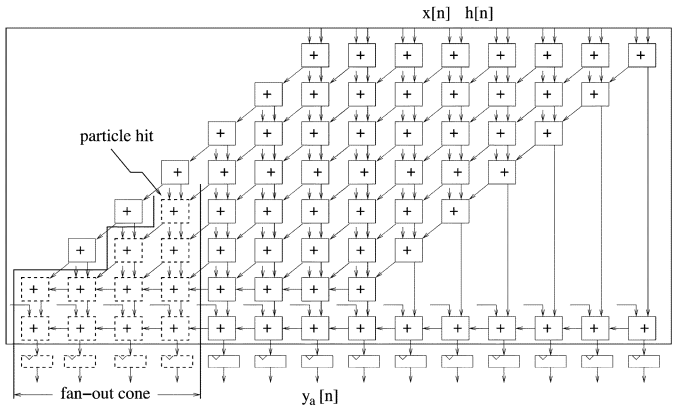

Fig. 1. Illustration of a soft error event in a multiply-and-accumulate (MAC) block. The blocks within the fan-out cone of the node hit by a particle can have erroneous outputs.

Lemma 1: If the flip vector $\boldsymbol{f}[n]$ is mutually independent and uniformly distributed, then the probability distribution function (pdf) of the soft error signal $\gamma[n]$ is given by

$$f_\Gamma(\gamma) \sim \frac{p_e}{4}(2-|\gamma|) + (1-p_e)\delta(\gamma), \quad \gamma \in (-2,2) \tag{5}$$

if $y_o[n]$ is uniformly distributed and

$$f_\Gamma(\gamma) \sim \frac{p_e}{2} Q\left(\frac{|\gamma|-1}{\sigma}\right) + (1-p_e)\delta(\gamma), \quad \gamma \in (-2,2) \tag{6}$$

if $y_o[n]$ is zero mean Gaussian with variance σ^2, where $Q(x) = (1/2\pi)\int_x^\infty \exp(-(u^2/2))du$ and p_e is the probability of soft error in the **M** block. Note that p_e is distinct from $P_{\rm er}$, which is the soft error probability of the whole system.

Proof: See Appendix A. ■

From (5) and (6), we see that $\gamma[n]$ is centered around zero.

B. Past Works

Redundancy-based techniques have been popularly employed in fault-tolerant computing systems [17]–[20]. Redundancy is introduced either via recomputation [17], code replication in software [18], or self-checking systems [19]. TMR [20], [28] is a well-known and commonly employed technique in high-end server-based systems [see Fig. 2(a)]. TMR includes three identical **M** blocks and employs majority voting to detect and correct errors. Since it is unlikely that two **M** blocks will be in error at the same time, TMR is effective in reducing the impact of soft errors. Although TMR is intuitively simple and easy to implement, it has a large area and power penalty.

In recent years, the ANT technique [23]–[25] has emerged as an attractive choice for enhancing the robustness of signal processing systems. As shown in Fig. 2(b), ANT-based systems employ a low-complexity (typically less than 10% of the **M** block complexity) estimator that approximately computes an estimate $y_e[n]$ of the error-free **M** block output $y_o[n]$. The estimator output $y_e[n]$ is compared to $y_a[n]$. If the Euclidean metric $d^E(y_a[n], y_e[n]) = |y_a[n] - y_e[n]|$ is greater than a prespecified

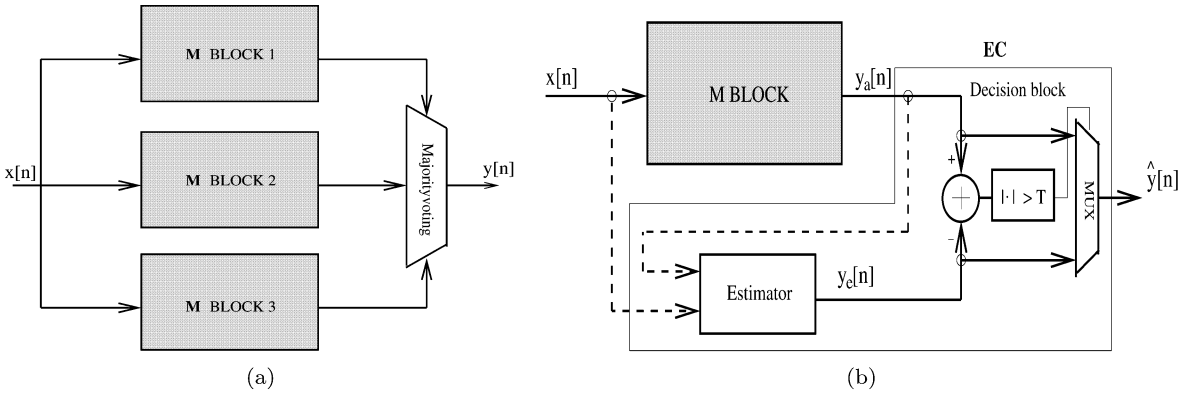

Fig. 2. Error/fault-tolerance techniques: (a) TMR and (b) ANT.

threshold T_h, then $y_e[n]$ is used as the corrected final output $\hat{y}[n]$. Otherwise, $y_a[n]$ is chosen as the final output $\hat{y}[n]$.

Unlike TMR, ANT techniques introduce a nonzero, but small and controllable error referred to as estimation noise $\epsilon[n] = y_o[n] - y_e[n]$. This is because the estimator output is an approximation of $y_o[n]$. This estimation error can be controlled by slightly overdesigning the **M** block. It has been shown that the combination of a slightly overdesigned **M** and **EC** block is effective in the presence of random errors [23]–[25] provided the **EC** block is error-free. Note, however, that the ANT technique cannot be directly applied to the soft-error problem because particle hits can occur in the estimator as well.

III. ASET

In this section, we assume the SEU model where any but at most one internal node in the **M** block or estimator can have its logic state flipped in a clock period. We assume that detection unit and memory block storing filter coefficient and input stream are properly protected by majority voting logic and ECC. We employ TMR as a benchmark for comparison. As mentioned, TMR can perfectly detect and correct SEUs. Hence, the signal-to-noise ratio (SNR) of a TMR-based system $(\mathrm{SNR}_{\mathrm{tmr}})$ will equal the desired $\mathrm{SNR}\,(\mathrm{SNR}_{\mathrm{des}})$. However, for many applications, TMR may not be practical due to the 3X complexity of the original system.

A. Spatial Aset (S-ASET)

Fig. 3(a) shows the block diagram of the proposed spatial ASET (S-ASET) technique. In addition to the **M** block, there are two estimators **E1** and **E2** in the **EC** block. In essence, S-ASET is the spatial diversity scheme based on M block estimator **E1** and **E2**. The **M** block executes most of the computations while the **EC** block detects and corrects errors. Fig. 3(b) shows the schedule followed by S-ASET. The decision block compares the **M** block output $y_a[n]$ and the first estimator output $y_{e1}[n]$. If $d^E(y_a[n], y_{e1}[n])$ is smaller than T_h, then $y_a[n]$ is chosen as the output. Otherwise, an additional comparator checks if the outputs of **E1** and **E2** are equal, i.e., $y_{e1}[n] = y_{e2}[n]$. If they are equal, an **M** block error is declared, otherwise, an estimator error is declared. In case of **M** block error, we choose $\hat{y}[n] = y_{e2}[n]$. Otherwise, we choose $\hat{y}[n] = y_a[n]$. The error control in S-ASET can be summarized as follows:

$$\hat{y}[n] = \begin{cases} y_a[n], & \text{if } d^E(y_a[n], y_{e1}[n]) \le T_h \\ y_a[n], & \text{if } d^E(y_a[n], y_{e1}[n]) > T_h \\ & \text{and } d^H(y_{e1}[n], y_{e2}[n]) = 1 \\ y_{e2}[n], & \text{if } d^E(\,y_a[n], y_{e1}[n],\,) > T_h \\ & \text{and } d^H(y_{e1}[n], y_{e2}[n]) = 0 \end{cases} \tag{7}$$

where $d^H(y_{e1}[n], y_{e2}[n])$ is the Hamming distance between $y_{e1}[n]$ and $y_{e2}[n]$ defined as

$$d^H(y_{e1}[n], y_{e2}[n]) = \cup_i (y^i_{e1}[n] \oplus y^i_{e2}[n]) \tag{8}$$

where $y^i_{e1}[n]$ and $y^i_{e2}[n]$ are the ith bits of $y_{e1}[n]$ and $y_{e2}[n]$, respectively, and $\oplus$ denotes the exclusive-OR operation. As **E1** and **E2** have a complexity that is less than 10% of that of the **M** block, the S-ASET complexity is roughly 1.2X of the original system, which is much lower than the complexity of TMR.

B. Spatio-Temporal Aset (ST-ASET)

The S-ASET scheme needs both estimators to be active in every clock cycle. Fig. 4(a) shows the block diagram of the spatio-temporal ASET (ST-ASET) technique that reduces power further. The key idea in ST-ASET is to employ **E1** (spatial redundancy) for monitoring an error and **E2** only when an error occurs but in the next clock cycle (temporal redundancy). Thus, **E2** is turned off most of the time if the errors are infrequent. As illustrated in Fig. 4(a), a pipeline cutset partitions the operation of the **EC** block into two phases: 1) error detection phase and 2) error correction phase.

Fig. 4(b) shows the schedule followed by ST-ASET. In the error detection phase, the **EC** block compares the **M** block output and **E1** output. If an error is detected in the nth cycle, i.e., $d^E(y_a[n], y_{e1}[n]) > T_h$, then **E2** is activated and an additional comparison is performed in the $n+1$th cycle to determine the erroneous block. If $d^H(y_{e1}[n], y_{e2}[n+1]) = 0$, we choose

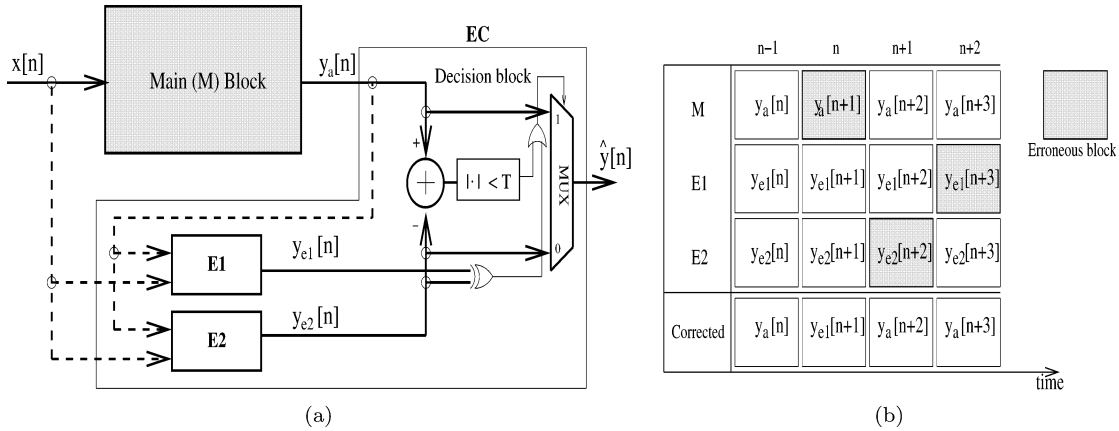

Fig. 3. S-ASET: (a) block diagram and (b) schedule.

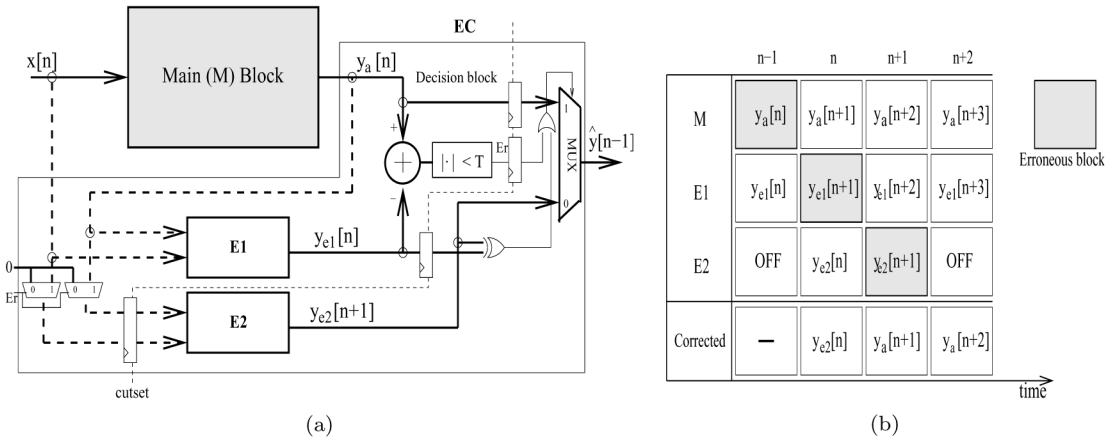

Fig. 4. ST-ASET: (a) block diagram and (b) schedule.

$\hat{y}[n] = y_{e2}[n+1]$. Otherwise, we choose $\hat{y}[n] = y_a[n]$. The decision rule of ST-ASET is described by

$$\hat{y}[n] = \begin{cases} y_a[n], & \text{if } d^E(y_a[n], y_{e1}[n]) \le T_h \\ y_a[n], & \text{if } d^E(y_a[n], y_{e1}[n]) > T_h \\ & \text{and } d^H(y_{e1}[n], y_{e2}[n+1]) = 1 \\ y_{e2}[n+1], & \text{if } d^E(y_a[n], y_{e1}[n]) > T_h \\ & \text{and } d^H(y_{e1}[n], y_{e2}[n+1]) = 0. \end{cases} \tag{9}$$

In (9), the only scenario where the error is detected but is uncorrected is when the main block is in error and **E2** is also in error in the next cycle. However, this situation is unlikely when $p_e \ll 1$. Hence, the performance of the ST-ASET is similar to the S-ASET.

C. Temporal Aset (T-ASET)

When the error rate is very small, as is in the case of soft error events, the probability of two consecutive errors in the estimator becomes very small. Thus, we can use a single estimator **E1** for both error detection and error correction purposes as shown in Fig. 5. The decision rule for temporal ASET (T-ASET) is described in (10). Compared with spatial or spatio-temporal ASET, the reduction of area in T-ASET scheme is considerable. As **E1** needs to be active all the time for error detection purposes, the power dissipation of the T-ASET is similar to that of the ST-ASET technique

$$\hat{y}[n] = \begin{cases} y_a[n], & \text{if } d^E(\, y_a[n], y_e[n]) \le T_h \\ y_a[n], & \text{if } d^E(y_a[n], y_e[n]) > T_h; \\ & d^H(y_e[n], y_e[n+1]) = 1 \\ y_e[n+1], & \text{if } d^E(y_a[n], y_e[n]) > T_h; \\ & d^H(y_e[n], y_e[n+1]) = 0. \end{cases} \tag{10}$$

D. Estimator

In this subsection, we review two estimator algorithms employed in ASET for error detection and correction. The role of the estimator is to generate $y_e[n]$ which is close to error-free **M** block output $y_o[n]$ with low complexity.

A) Reduced Precision Redundancy (RPR): An RPR estimator [25] employs a replica of the **M** block with reduced precision arithmetic units. The RPR estimator output $y_{e,\mathrm{rpr}}[n]$ is given by

$$y_{e,\mathrm{rpr}}[n] = \sum_{k=0}^{N-1} h_r[k] x_r[n-k] \tag{11}$$

where $h_r[n]$ and $x_r[n]$ are the truncated versions of the **M** block filter coefficient and input, respectively. When an error is de-

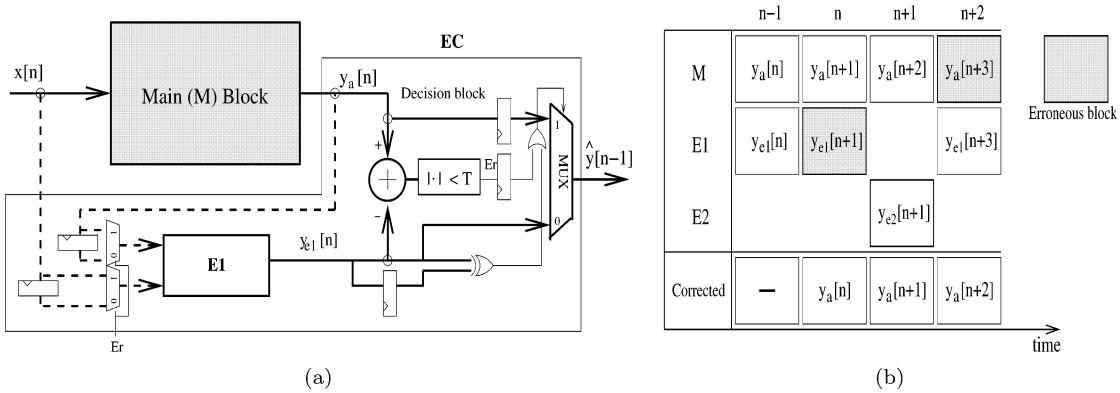

Fig. 5. T–ASET: (a) block diagram and (b) schedule.

tected using (8)–(10), $y_{e,\mathrm{rpr}}[n]$ is employed as the final output. Reasonable choice of replica precision can minimize the quantization noise since the frequency of error is usually small. Since the quantization noise is insensitive to the bandwidth, RPR can be employed for a wide range of filter bandwidths.

B) Predictor: A prediction-based estimator [23] employs a low-complexity forward predictor to estimate the current filter output $y_o[n]$ from the past **M** block outputs $y_o[n-k], k>0$. The consecutive outputs of the **M** block are highly correlated for narrowband filters. Hence, an N_p-tap predictor can generate an estimate $y_{e,\mathrm{prd}}[n]$ to be used as the corrected output when an error is detected. The output of an N_p-tap forward predictor is

$$y_{e,\mathrm{prd}}[n] = \sum_{k=0}^{N_p-1} h_p[k] y_a[n-k-1] \tag{12}$$

where $h_p[n]$ is obtained via the Wiener–Hopf equation [27]. The predictor performs well for narrowband filters (bandwidth is less than $0.5f_s$, where f_s is the sampling frequency) and in environments with a frequency of errors less than 10^{-3}.

IV. ASET Performance Analysis

In Section III, we saw that ASET involves computing the outputs of the **M** block, the two estimators followed by comparisons between these outputs with respect to a threshold T_h. The overall SNR achieved by ASET $(\mathrm{SNR}_{\mathrm{aset}})$ is, therefore, a function of the raw error frequency p_e and the decision threshold T_h. In this section, we investigate this relationship between the SNR, T_h, and p_e.

The uncorrected output $y_a[n]$ and the corrected output $\hat{y}[n]$ in ASET can be written as

$$y_a[n] = d[n] + \eta[n] + \gamma[n] \tag{13}$$
$$\hat{y}[n] = d[n] + \eta[n] + \gamma_r[n] \tag{14}$$

where $\gamma_r[n]$ is the residual soft error signal.

In order to meet a specific desired $\mathrm{SNR}(\mathrm{SNR}_{\mathrm{des}}), \mathrm{SNR}_{\mathrm{aset}}$ needs to satisfy the following inequality:

$$\mathrm{SNR}_{\mathrm{aset}} = 10\log_{10}\frac{\sigma_d^2}{\sigma_\eta^2+\sigma_{\gamma_r}^2} \geq \mathrm{SNR}_{\mathrm{des}} \tag{15}$$

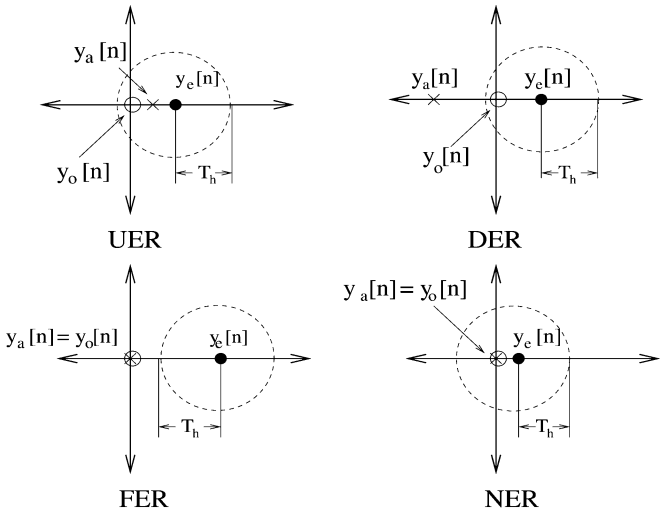

Fig. 6. Four possible decisions in ANT and ASET scheme.

where σ_d^2 and σ_η^2 are the powers of desired signal $d[n]$ and channel noise $\eta[n]$, respectively, and $\sigma_{\gamma_r}^2$ is the power of $\gamma_r[n]$. Equation (15) can be rewritten as

$$\sigma_d^2 \cdot 10^{-\frac{\mathrm{SNR}_{\mathrm{des}}}{10}} \geq \sigma_\eta^2 + \sigma_{\gamma_r}^2. \tag{16}$$

Equation (16) indicates that the effect on system performance is minimal if the residual soft error power is much smaller than the channel noise power.

A. rMSE Analysis

The decision rule of spatial ASET in Section III-A results in four possible decision events as shown in Fig. 6. Without loss of generality, we focus on the **M** block being in error with probability p_e. In the following, we assume that Y_a, Y_e, Y_o and $\hat{Y}$ are random variables representing $y_a[n], y_e[n], y_o[n], \hat{y}[n]$, respectively, with the time index n dropped due to notational convenience. The soft error $\gamma[n]$ can go undetected if it is small enough, i.e., the distance metric $d^E(y_a[n], y_{e1}[n])$ is less than or equal to T_h. Such an undetected error event (UER) appears with a probability P_{uer} given by

$$P_{\mathrm{uer}} = P_r(|Y_a - Y_e| \leq T_h, Y_a \neq Y_o). \tag{17}$$

The UER event results in the final output being $\hat{y}[n] = y_a[n]$. If $\gamma[n]$ is large enough, soft error is detected, i.e., $d^E(y_a[n], y_{e1}[n]) > T_h$. The resulting detected error event (DER) results in the $\hat{y}[n] = y_e[n]$ with probability

$$P_{\text{der}} = P_r(|Y_a - Y_e| > T_h, Y_a \neq Y_o). \tag{18}$$

In the absence of errors, i.e., no error event (NER) where $\gamma[n] = 0$, the output is chosen as $\hat{y}[n] = y_a[n] = y_o[n]$. However, if the threshold T_h is too small such that it is less than the magnitude of estimation error $\epsilon[n]$, where $\epsilon[n]$ is given by

$$\epsilon[n] = y_o[n] - y_e[n] \tag{19}$$

then a false alarm error event (FER) occurs. In such a case, $y_e[n]$ is incorrectly chosen as the output. The probability of the FER event is given by

$$P_{\text{fer}} = (1 - p_e)P_r(|Y_o - Y_e| > T_h). \tag{20}$$

The following theorem describes rMSE of an ASET based system.

Theorem 2: The residual soft error power $\sigma^2_{\gamma_r} = E[|Y_o - \hat{Y}|^2]$ is given by

$$\sigma^2_{\gamma_r} = P_{\text{der}} \cdot \sigma^2_{\text{der}} + P_{\text{uer}} \cdot \sigma^2_{\text{uer}} + P_{\text{fer}} \cdot \sigma^2_{\text{fer}} \tag{21}$$

where

$$\begin{aligned}
P_{\text{uer}} &= P_r(|Y_a - Y_e| \leq T_h, Y_a \neq y_o) \\
P_{\text{der}} &= P_r(|Y_a - Y_e| > T_h, Y_a \neq y_o) \\
P_{\text{fer}} &= (1 - p_e)P_r(|Y_o - Y_e| > T_h) \\
\sigma^2_{\text{uer}} &= E\left[|Y_o - Y_a|^2 | |Y_a - Y_e| \leq T_h\right] \\
\sigma^2_{\text{der}} &= E\left[|Y_o - Y_e|^2 | |Y_a - Y_e| > T_h\right] \\
\sigma^2_{\text{fer}} &= E\left[|Y_o - Y_e|^2 | |Y_o - Y_e| > T_h\right].
\end{aligned}$$

Proof: See Appendix B. ∎

Theorem 2 indicates that $\sigma^2_{\gamma_r}$ depends on the following: 1) raw probability of error p_e; 2) the effectiveness of the estimator being employed; and 3) the decision threshold T_h. From (16) and (21), we obtain the following inequality:

$$\sigma_d^2 10^{-\frac{\text{SNR}_{\text{des}}}{10}} - \sigma_\eta^2 > P_{\text{der}}\sigma^2_{\text{der}} + P_{\text{uer}}\sigma^2_{\text{uer}} + P_{\text{fer}}\sigma^2_{\text{fer}}. \tag{22}$$

B. Optimum rMSE

In this subsection, we find out the probability and noise power of each event in (22) and present a detailed rMSE analysis. We employ the soft error model in Section II-A and further assume that the estimation error $\epsilon[n]$ is uniform over a sufficiently small region around zero.

First, in case of DER event, we trivially obtain $\sigma^2_{\text{der}} \sim \sigma^2_\epsilon$ since $|y_a[n] - y_e[n]| > T_h, y_a[n] \neq y_o[n]$ case occurs with high probability.

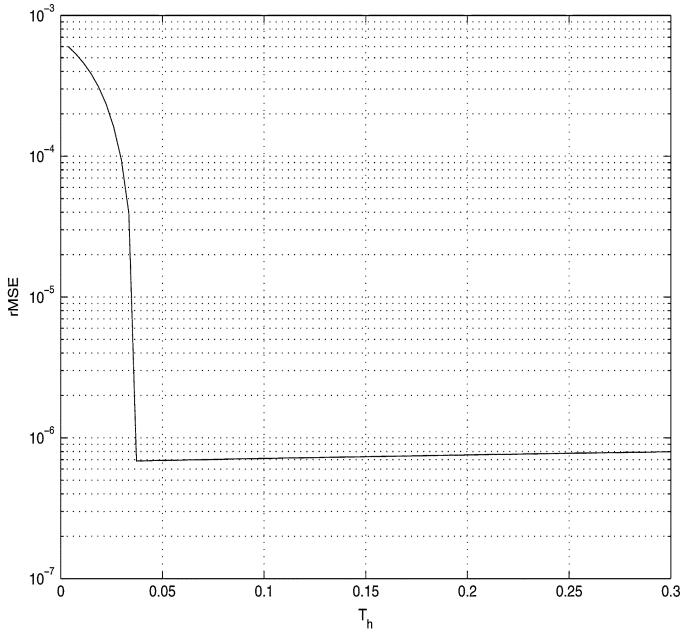

Fig. 7. Residual soft error power $\sigma^2_{\gamma_r}$ versus T_h.

Lemma 3: If $y_o[n]$ is uniform and Gaussian distributed, then the noise power in the UER event defined in (22) is given by

$$P_{\text{uer}} \sim \begin{cases} p_e\left(T_h - \frac{1}{4}\left(T_h^2 + \sigma_\epsilon^2\right)\right) & \text{Uniform} \\ \frac{1}{2}p_e T_h & \text{Gaussian} \end{cases} \tag{23}$$

$$\sigma^2_{\text{uer}} \sim \sigma^2_\epsilon + \frac{1}{3}T_h^2. \tag{24}$$

Proof: See Appendix C. ∎

The result in Lemma 3 is consistent with our expectation that the probability of the UER event increases with threshold T_h. Note further that σ^2_{uer} varies quadratically with T_h and is always greater than σ^2_{der}.

Assuming ϵ is uniformly distributed, one can easily show that P_{fer} and σ^2_{fer} are, respectively

$$\begin{aligned}
P_{\text{fer}} &= (1 - p_e)P_r(|\epsilon| > T_h) = (1 - p_e)\left(\frac{\epsilon_{\max} - T_h}{\epsilon_{\max}}\right) \\
\sigma^2_{\text{fer}} &= E[|Y_o - Y_e|^2 | |Y_o - Y_e| > T_h] \\
&= E[\epsilon^2 | |\epsilon| > T_h] \\
&\sim \frac{1}{3}(\epsilon^2_{\max} - \frac{T_h^3}{\epsilon_{\max}})
\end{aligned} \tag{25}$$

where $\epsilon_{\max} = \max_{\forall y_o[n]} |y_o[n] - y_e[n]|$ and $\epsilon_{\max} \geq T_h$ is assumed. With these, we are now able to determine an expression for the threshold T_h^* that minimizes $\sigma^2_{\gamma_r}$.

Theorem 4: The optimum threshold that minimizes the residual soft error power $\sigma^2_{\gamma_r}$ of ASET is given by

$$T_h^* = \epsilon_{\max}. \tag{26}$$

Proof: See Appendix D. ∎

As an example, for the case of a 30-tap FIR filter ($\omega_c = 0.2\pi$) with 16-bit MDSP and 8-bit replica estimator, the residual soft error power for different values of the threshold T_h is shown in Fig. 7. When the $T_h < T_h^*$, residual soft error power increases abruptly due to a rapid increase in P_{fer}. Whereas, when

$T_h > T_h^*$, residual soft error power increases gradually due to the moderate increase in P_{uer}. If we choose T_h to be greater than T_h^* only DER and UER events contribute to the noise power as indicated by Theorem 4. Hence, (21) can be simplified to

$$\sigma_{\gamma_r}^2 = P_{\text{der}}\sigma_\epsilon^2 + P_{\text{uer}}\sigma_{\text{uer}}^2. \tag{27}$$

Further, by substituting (23) in (28), we obtain

$$\sigma_{\gamma_r}^2 \sim p_e\sigma_\epsilon^2 + \frac{1}{3}P_{\text{uer}}\epsilon_{\max}^2. \tag{28}$$

It is interesting to note that the two terms in (28) represent the effectiveness of error correction and error detection, respectively. In case of TMR, which is an extreme form of S-ASET, $\sigma_\epsilon^2 = 0$ and $P_{\text{uer}} = 0$ and, hence, $\sigma_{\gamma_r}^2 = 0$.

As mentioned in Section III-B, the residual soft error power of S-ASET in (28) does not hold for ST-ASET and T-ASET. When an error occurs in two consecutive time units, say $n+1$ in MDSP and $n+2$ in **E2**, the error control in ST-ASET will fail. In case of T-ASET, error detection in previous cycle prohibits error control in the current cycle. Considering these factors, the residual soft error powers of ST-ASET and T-ASET are given by

$$\sigma_{\gamma_r}^2 = P'_{\text{der}}\sigma_\epsilon^2 + P'_{\text{uer}}\sigma_{\text{uer}}^2 + p'_e p_e \sigma_\eta^2 \tag{29}$$

where $P'_{\text{der}} = (1-p'_e)P_{\text{der}}$, $P'_{\text{uer}} = (1-p'_e)P_{\text{uer}}$, and p'_e is the probability of error in **E1** and **E2** for ST-ASET and $P_r(|y_a[n] - y_e[n]| > T_h)$ for T-ASET. Since $p'_e p_e$ is very small in general, the asymptotic performance of spatio-temporal and temporal ASET are similar to the spatial ASET when $p_e \ll 1$. Indeed, as shown in Fig. 8, employing the setup of Fig. 7, the residual soft error power of spatio-temporal ASET is found to be close to that of spatial ASET when $p_e < 10^{-3}$. In any case, as is clearly observed from Fig. 8, the residual soft error power of ASET is sufficiently small for a wide range of p_e thereby making it possible to achieve the desired performance.

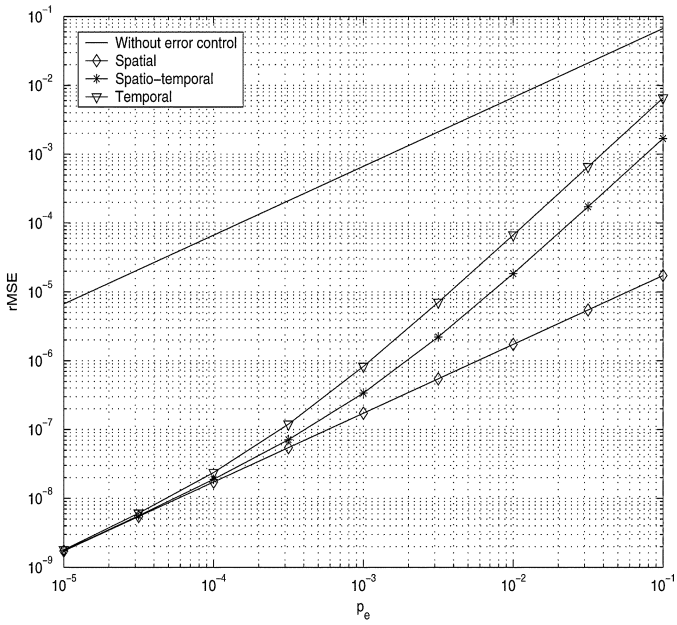

Fig. 8. Residual soft error power $\sigma_{\gamma_r}^2$ of spatial, spatio-temporal, and temporal ASET versus p_e.

V. Discussion and Simulation Results

In this section, we study the performance and power savings of the proposed ASET techniques over the original system (no error control), ANT, and TMR in the context of frequency selective filtering. In all simulations, we employ RPR scheme as an estimator for ASET. We first describe the simulation setup and then present the simulation results.

A. Simulation Setup

Fig. 9 illustrates the system being considered. The **M** block is a filter that extracts a signal $d_1[n]$ in the presence of other signals $d_2[n], d_3[n]$, white Gaussian noise source $\eta[n]$, and soft error signal $\gamma[n]$. As mentioned earlier, we consider four cases. These are when the **M** block is an FIR filter and employs: 1) no error protection; 2) TMR; 3) ANT; and 4) ASET techniques.

Soft Error Generation and Injection: In order to emulate the realistic single event upset environment, we implemented a gate-level multiplier-and-accumulator (MAC). When a particle hit occurs, a randomly selected internal node output is flipped and so are the outputs of all the gates in the fan-out cone of that node. The particle hit can occur either in the **M** block or the estimator. Assuming the probability of error in the entire system

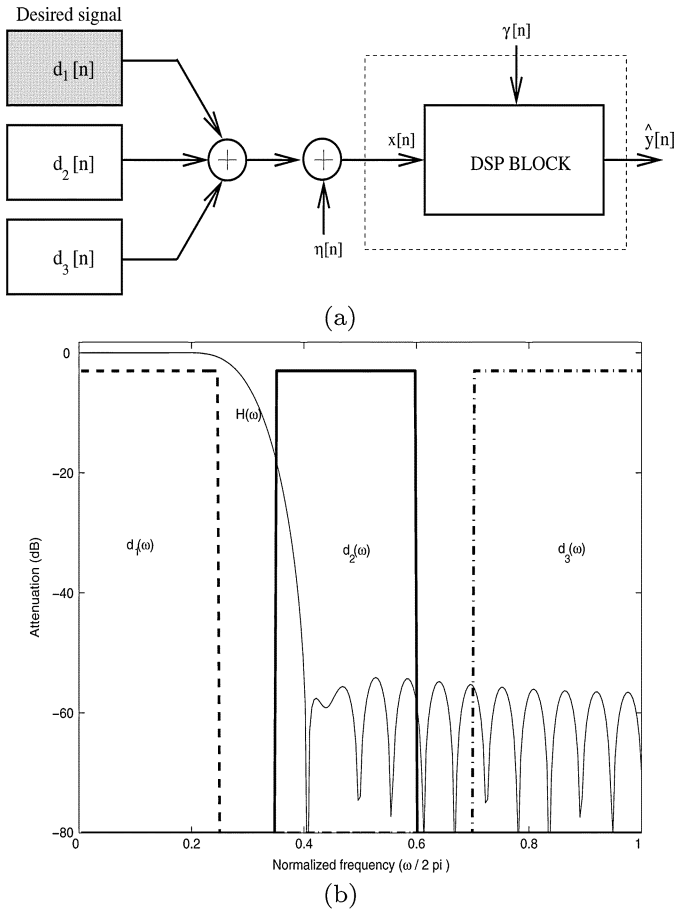

Fig. 9. Simulation setup for ASET: (a) ASET frequency selective filter and (b) frequency response of $d_i[n]$ and $h[n]$.

to be $P_{\rm er}$, the probability of error in the **M** block p_e and each estimator $p_{\rm est}$ of ASET are given by

$$p_e = P_{\rm er}\left(\frac{A_{\rm mdsp}}{A_{\rm mdsp}+A_{\rm est}}\right) \tag{30}$$

$$p_{\rm est} = P_{\rm er} - p_e = P_{\rm er}\left(\frac{A_{\rm est}}{A_{\rm mdsp}+A_{\rm est}}\right) \tag{31}$$

where $A_{\rm mdsp}$ and $A_{\rm est}$ are the areas of the **M** block and estimator, respectively. In case of S-ASET and ST-ASET, $A_{\rm est} = A_{E1}+A_{E2}$ and $A_{\rm est} = A_{E1}$ for T-ASET, where A_{E1} and A_{E2} are the areas of **E1** and **E2**, respectively.

System Specifications: Each signal $d_i[n]$ used in our simulation has a bandwidth of 0.25π with a guard band of 0.1π. In addition, a Gaussian noise with a power spectral density -30 dB below the signal level is added at the receiver. In order to extract the desired signal, a Parks–McClellan FIR low-pass filter is employed [30].

The error-free desired output SNR ($\rm SNR_{des}$) and SNR of the four techniques ($\rm SNR_{act}$) are given by

$$\rm SNR_{des} = 10\log_{10}\frac{\sigma_d^2}{\sigma_{d-y_o}^2} \tag{32}$$

$$\rm SNR_{act} = 10\log_{10}\frac{\sigma_d^2}{\sigma_{d-\hat{y}}^2} \tag{33}$$

where $\sigma_{d-y_o}^2 = E[|d-y_o|^2]$ and $\sigma_{d-\hat{y}}^2 = E[|d-\hat{y}|^2]$.

We assume $\rm SNR_{des} = 25$ dB, where the **M** block is designed to have a 0.5 dB margin for all techniques except TMR. Note that TMR is designed without any margin because it can perfectly correct errors under the SEU assumption. The original **M** block can provide this SNR with a 33-tap (30-tap in case of TMR) filter along with 16-bit multiplier. The replica estimator employs 8-bit multiplier with the same number of taps as the **M** block.

B. Simulation Results

Fig. 10 shows the output SNRs for all the techniques. We see that the final output SNR for the system with no error control drops severely (22 dB) as $P_{\rm er}$ increases from 10^{-6} to 10^{-1}. Note that the SNR loss becomes significant (>5 dB if $P_{\rm er} \geq 10^{-2}$) for ANT because the error control fails when soft errors occur in the estimator. All ASET techniques maintain the SNR until $P_{\rm er}$ approaches 10^{-3} after which the performance of ST-ASET and T-ASET begins to drop in high error regime $P_{\rm er} > 10^{-3}$. However, S-ASET maintains the algorithmic performance up to $P_{\rm er} = 10^{-2}$ providing more than three orders of magnitude improvement in soft error tolerance over the original MDSP with no error control.

In order to observe the residual noise distribution conditioned on error occurrence, we plotted $P(\gamma_r|er)$ in Fig. 11 when $P_{\rm er} = 10^{-2}$. Note that it is hard to distinguish the difference in ASET schemes when $P_{\rm er} < 10^{-2}$. We observe that the distribution of the original scheme with no error control is wide in the range $(-2, 2)$. Since ANT cannot correct soft errors perfectly, it also has a wide residual noise distribution. However, the residual noise of S-ASET is centered around 0. Even though there are high magnitude errors in ST-ASET and T-ASET, these occur rarely and, therefore, the effect of residual noise power on the overall performance is negligible.

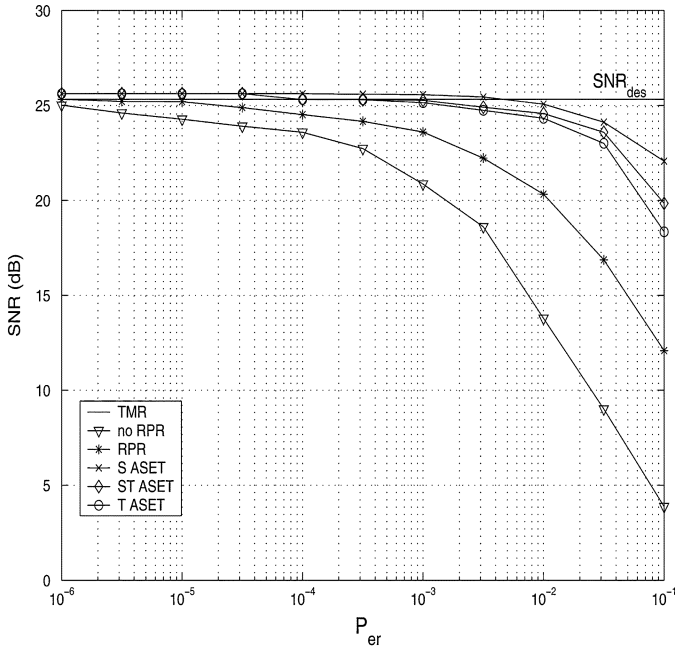

Fig. 10. SNR performance of ASET schemes versus $P_{\rm er}$ in SEU environment.

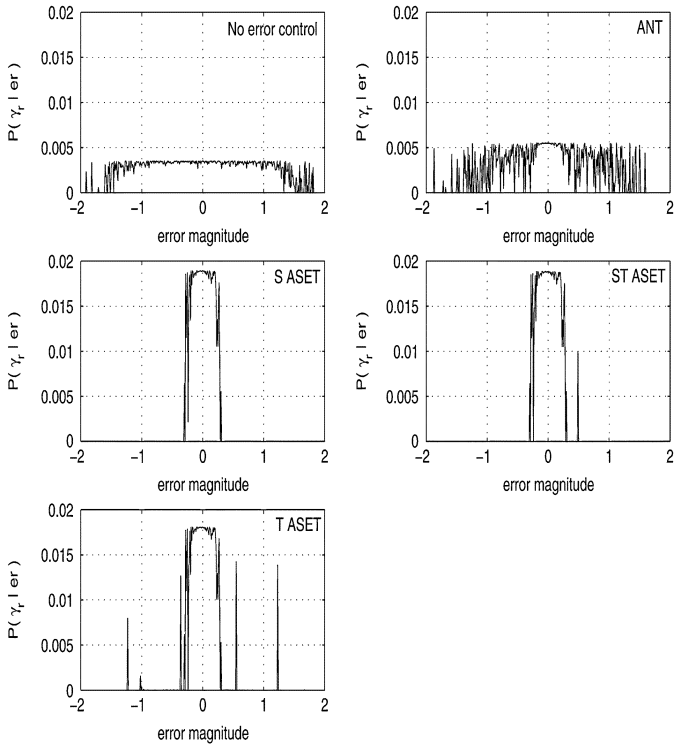

Fig. 11. Residual noise distribution of ASET schemes.

C. Power Savings

In order to evaluate the power savings of the proposed techniques over the TMR technique, we searched the precision of

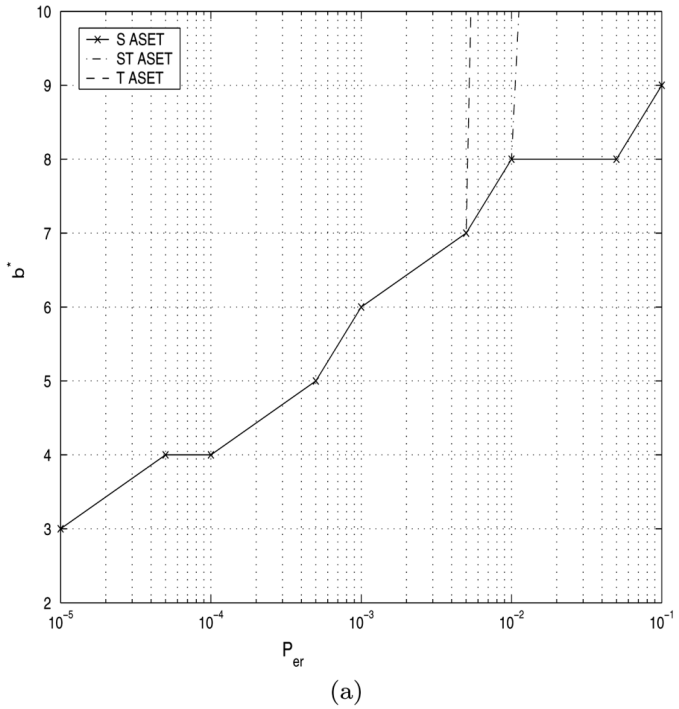

(a)

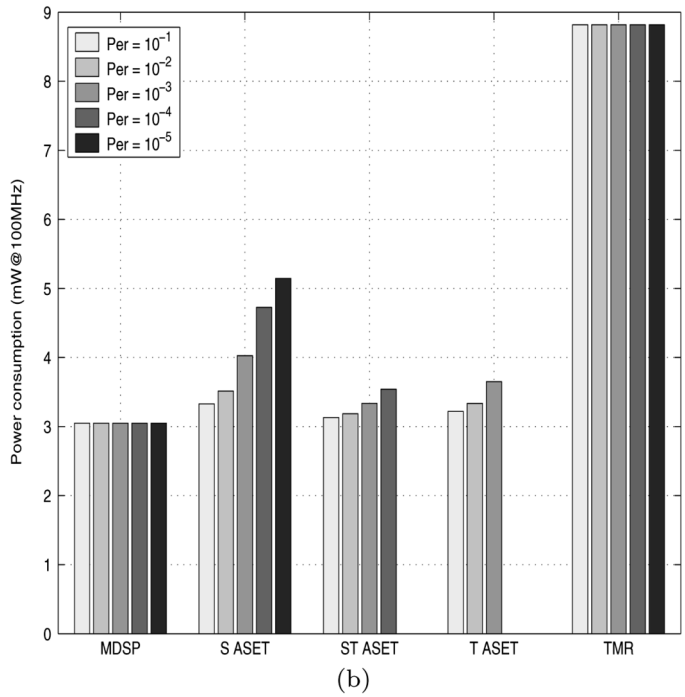

(b)

Fig. 12. Power analysis of ASETs: (a) b^* versus $P_{\rm er}$ and (b) the power dissipation for $P_{\rm er}$ variation.

replica (b_r) for each value of $P_{\rm er}$. The optimum precision b_r^* satisfying system requirements is given by

$$b_r^* = \arg\min_{b_r} \left(\sigma_d^2 \cdot 10^{-\frac{\rm SNR_{dB}}{10}} - \sigma_\eta^2 > \sigma_{\gamma_r}^2(b_r) \right). \qquad (34)$$

Fig. 12(a) shows the optimum precision of replica estimator as a function of $P_{\rm er}$. As $P_{\rm er}$ increases, the estimation noise σ_ϵ^2 needs to be reduced to satisfy desired performance and, hence, the precision of ASET increases. Since the spatio-temporal and temporal ASETs do not satisfy the system requirements in high $P_{\rm er}$ regime $(P_{\rm er} > 10^{-2})$, the spatial ASET becomes the only option in this region.

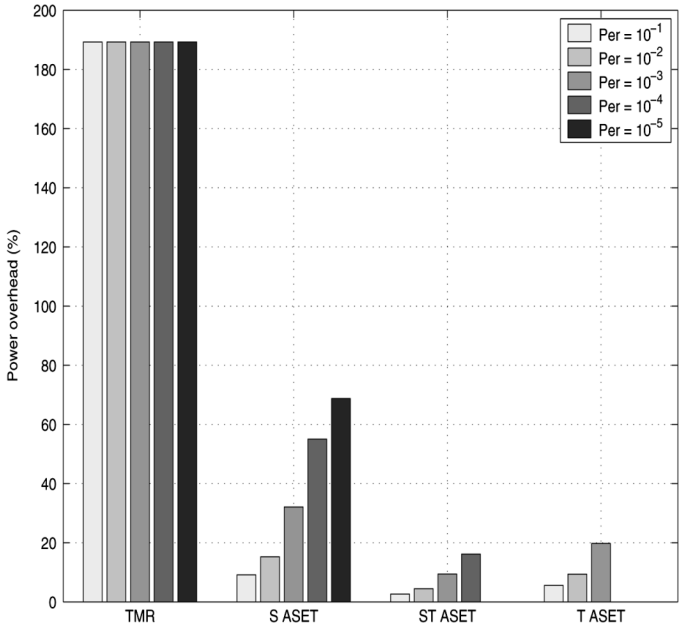

Fig. 13. Power overhead versus $P_{\rm er}$.

With the optimum precision thus obtained, we compared the power consumption for ASET and TMR. In order to do this, we designed each system in Section V-A using VHDL and obtained the power estimate via *Synopsys Design Analyzer* employing a 0.18-μm standard cell library. As shown in Fig. 12(b), the power consumption of TMR is roughly $3\mathbf{X}$ of **M** block while the proposed ASETs have similar power consumption as **M** block in low $P_{\rm er}$. Though the power consumption of ASETs increases with $P_{\rm er}$, the amount of increase is small particularly for ST-ASET and T-ASET.

We next computed the power overhead of the proposed ASET scheme. The power overhead $P_{\rm ovh}$ of the proposed ASET scheme is given by

$$P_{\rm ovh} = \frac{P_{\rm aset} - P_M}{P_M} \times 100\% \qquad (35)$$

where P_M and $P_{\rm aset}$ are the power dissipation of the **M** block and ASET, respectively. The resulting $P_{\rm ovh}$ as a function of $P_{\rm er}$ is shown in Fig. 13. We see that the proposed ASET techniques have much smaller overhead than the TMR. In particular, since **E2** in ST-ASET and T-ASET is activated infrequently, the overhead is smaller ($< 10\%$) than that for S-ASET in low $P_{\rm er}$ region.

VI. Conclusion

In this paper, we presented an algorithmic approach toward soft error-tolerance for signal processing systems referred to as ASET. The proposed approach employs two estimators which work in tandem with a main block to detect and correct errors. The proposed approach has an area and power overhead that is 2X smaller than that of the popular TMR technique. This work opens up new areas of research in which the tradeoffs between soft error-tolerance and power can be explored at the algorithmic level. For

example, future work could be directed toward studying the impact of voltage scaling and ASET on the soft error-rates. The **M** block could be voltage overscaled [25] to reduce power further and the estimators could be used to detect and correct the errors. Our recent work [32] has shown that soft error-rates in combinational logic are a weak function of the supply voltage. Hence, low-voltage ASET systems seem to be promising. Another direction of exploration would be to extend ASET solution to general purpose processors. Since the estimator can be realized with a small and power efficient arithmetic unit, ASET solution combined with appropriate ECC can be effective in signal processing application realized by general purpose processors.

Appendix A
Proof of Lemma 1

From (6) and (4), the probability of soft error can be written as

$$\begin{aligned} P_r(\Gamma=\gamma) &= P_r(Y_a - Y_o = \gamma) \\ &= P_r(F \oplus Y_o - Y_o = \gamma) \\ &= \sum_i \sum_j P_r(Y_o = y_i) P_r(F = f_j : \mathcal{A}) \end{aligned} \quad (36)$$

where $\mathcal{A} = \{f_j \oplus y_i = y_i + \gamma\}, Y_a, Y_o$, and Γ are the random variables corresponding to y_a, y_i, and γ, respectively, and F is the random variable corresponding to the 2's complement representation of flip vector $\boldsymbol{f}$. Since a PMF is well approximated by a continuous pdf if the precision N is sufficiently large [31], and F exists only when $-1 \le y_i + \gamma \le 1$, (36) can be rewritten as

$$P_r(\Gamma=\gamma) = \int_{-1}^{1} \int_{-1-\gamma}^{1-\gamma} f_{Y_o}(y) f_F(f)\, dy_o df. \quad (37)$$

By substituting $f_{Y_o}(y) = (1/2)$ and $f_F(f) = (p_e/2)$ in (37) and also noting that F has a point mass of $1 - p_e$ at $f = 0$ (no error occurs), (37) becomes

$$f_\Gamma(\gamma) \sim \frac{p_e}{4}(2 - |\gamma|) + (1 - p_e)\delta(\gamma),\ \gamma \in (-2, 2). \quad (38)$$

Substituting $f_{Y_o}(y) = 1/(\sqrt{2\pi}\sigma)\exp(-y^2/2\sigma^2)$ in (37), we get

$$f_\Gamma(\gamma) \sim \frac{p_e}{2} Q\left(\frac{|\gamma| - 1}{\sigma}\right) + (1 - p_e)\delta(\gamma),\ \gamma \in (-2, 2) \quad (39)$$

where $Q(x) = (1/2\pi)\int_x^\infty \exp(-(u^2/2))du$.

Appendix B
Proof of Theorem 2

As discussed in Section IV-B, there are four possible events in soft error detection. Therefore, the residual soft error power can be written as

$$\begin{aligned} \sigma^2_{\gamma_r} &= E[|Y_o - \hat{Y}|^2] \\ &= \int |y_o - \hat{y}|^2 f_{Y_o,\hat{Y}}(y_o, \hat{y}) dy_o d\hat{y} \\ &= \int\int_{|y_a - y_e| \le T_h, y_a \ne y_o} |y_o - y_a|^2 f_{Y_o Y_a}(y_o, y_a) dy_o dy_a \end{aligned} \quad (40)$$

$$+ \int\int_{|y_a - y_e| > T_h, y_a \ne y_o} |y_o - y_e|^2 f_{Y_o Y_a}(y_o, y_a) dy_o dy_a \quad (41)$$

$$+ (1 - p_e) \int_{|y_o - y_e| > T_h} |y_o - y_e|^2 f_{Y_o}(y_o) dy_o \quad (42)$$

$$+ (1 - p_e) \int_{|y_o - y_e| \le T_h} \underbrace{|y_o - y_o|^2}_{0} f_{Y_o}(y_o) dy_o. \quad (43)$$

Note that the point mass $f_{Y_a}(y_a)$ at $y_a = y_o$ is $1 - p_e$, where p_e is the **M** block error probability.

From the definition of conditional expected value [31], we have

$$E[g(x,y)|(x,y) \in \mathcal{A}] = \frac{\int_{\mathcal{A}} g(x,y) f_{X,Y}(x,y) dx dy}{\int_{\mathcal{A}} f_{X,Y}(x,y) dx dy}. \quad (44)$$

By denoting $\sigma^2_{\text{uer}} = E[|Y_o - Y_a|^2 | |Y_a - Y_e| \le T_h], P_{\text{uer}} = P_r(|Y_a - Y_e| \le T_h, Y_a \ne y_o)$ and also using (44), (40) can be rewritten as

$$\int\int_{|y_a - y_e| \le T_h, y_a \ne 0} |y_o - y_a|^2 f_{Y_o,Y_a}(y_o, y_a) dy_o dy_a = P_{\text{uer}} \sigma^2_{\text{uer}}. \quad (45)$$

Similarly, denoting $\sigma^2_{\text{der}} = E[|Y_o - Y_e|^2 | |Y_a - Y_e| > T_h]$ and $P_{\text{der}} = P_r(|Y_a - Y_e| > T_h, Y_a \ne y_o)$, (41) can be rewritten as

$$\int\int_{|y_a - y_e| \le T_h, y_a \ne 0} |y_o - y_a|^2 f_{Y_o,Y_a}(y_o, y_a) dy_o dy_a = P_{\text{der}} \sigma^2_{\text{der}}. \quad (46)$$

Finally, by denoting $P_{\text{fer}} = (1 - p_e) P(|Y_o - Y_e| > T_h)$ and $\sigma^2_{\text{fer}} = E[|Y_o - Y_e|^2 | |Y_o - Y_e| > T_h]$, the FER event can be rewritten as

$$(1 - p_e) \int_{|y_o - y_e| > T_h} |y_o - y_e|^2 f_{Y_o}(y_o) dy_o = P_{\text{fer}} \sigma^2_{\text{fer}}. \quad (47)$$

Therefore, by substituting (45), (46), and (47) into (40), we get

$$\sigma^2_{\gamma_r} = P_{\text{der}} \cdot \sigma^2_{\text{der}} + P_{\text{er}} \cdot \sigma^2_{\text{uer}} + P_{\text{fer}} \cdot \sigma^2_{\text{fer}}.$$

Appendix C
Proof of Lemma 3

Rewriting (22), we get

$$\begin{aligned} \sigma^2_{\text{uer}} &= E[|Y_o - Y_a|^2 | |Y_a - Y_e| \le T_h] \\ &= E[\gamma^2 | -T_h - \epsilon \le \gamma \le T_h - \epsilon] \\ &= \frac{\int_\epsilon \int_{-T_h-\epsilon}^{T_h-\epsilon} \gamma^2 f'_\Gamma(\gamma) f_{\mathcal{E}}(\epsilon) d\gamma d\epsilon}{\int_\epsilon \int_{-T_h-\epsilon}^{T_h-\epsilon} f'_\Gamma(\gamma) f_{\mathcal{E}}(\epsilon) d\gamma d\epsilon} \end{aligned} \quad (48)$$

where $\mathcal{E}$ and Γ are random variables corresponding to the estimation noise ϵ and soft error γ, respectively. In addition, we denote $f'_\Gamma(\gamma)$ to be the pdf of soft error when $\gamma \ne 0$. Indeed,

UER event occurs only when $\gamma \neq 0$. The denominator is given by [refer to (5)]

$$\int_{\epsilon} f_{\mathcal{E}}(\epsilon) \int_{-T_h-\epsilon}^{T_h-\epsilon} f'_{\Gamma}(\gamma) d\gamma d\epsilon = \int_{\epsilon} f_{\mathcal{E}}(\epsilon) p_e \left(T_h - \frac{1}{4}(T_h^2 + \epsilon^2) \right) d\epsilon. \quad (49)$$

Using the identities $\int_{\epsilon} f_{\mathcal{E}}(\epsilon) d\epsilon = 1$ and $\int_{\epsilon} \epsilon^2 f_{\mathcal{E}}(\epsilon) d\epsilon = \sigma_{\epsilon}^2$ in (49), we obtain

$$\int_{\epsilon} \int_{-T_h-\epsilon}^{T_h-\epsilon} f'_{\Gamma}(\gamma) f_{\mathcal{E}}(\epsilon) d\gamma d\epsilon = p_e \left(T_h - \frac{1}{4}\left(T_h^2 + \sigma_{\epsilon}^2\right) \right). \quad (50)$$

Note that (50) is an expression for P_{uer} [refer to (22)]. After manipulation, the numerator can be rewritten as

$$\int_{\epsilon} \int_{-T_h-\epsilon}^{T_h-\epsilon} \gamma^2 f'_{\Gamma}(\gamma) f_{\mathcal{E}}(\epsilon) d\gamma d\epsilon = p_e \left(\frac{1}{3} T_h^3 + T_h \sigma_{\epsilon}^2 - \frac{1}{8}\left(T_h^4 + \sigma_{\epsilon}^4 + 6 T_h^2 \sigma_{\epsilon}^2\right) \right) \quad (51)$$

where $\sigma_{\epsilon}^4 = \int_{\epsilon} \epsilon^4 f_{\mathcal{E}}(\epsilon) d\epsilon$. Substituting (50) and (51) into the (48), we get

$$\sigma_{\text{uer}}^2 = \frac{\frac{1}{3} T_h^3 + T_h \sigma_{\epsilon}^2 - \frac{1}{8}(T_h^4 + 6\, T_h^2 \sigma_{\epsilon}^2 + \sigma_{\epsilon}^4)}{T_h - \frac{1}{4}(T_h^2 + \sigma_{\epsilon}^2)} \sim \sigma_{\epsilon}^2 + \frac{1}{3} T_h^2 \quad (52)$$

where we exploit the fact that $T_h, \sigma_{\epsilon}^2 \ll 1$. When $y_o[n]$ is Gaussian, $f'_{\Gamma}(\gamma) \sim (p_e/2)$ around $\gamma = 0$. Following a similar procedure, one can show that the denominator and numerator in (48) are $(p_e/2) T_h$ and $(p_e/2)(T_h \sigma_{\epsilon}^2 + (1/3) T_h^3)$, respectively. Thus, we get

$$\sigma_{\text{uer}}^2 \sim \sigma_{\epsilon}^2 + \frac{1}{3} T_h^2. \quad (53)$$

Appendix D
Proof of Theorem 4

Recall that $\epsilon_{\max} = \max_{\forall y_o[n]} |y_o[n] - y_e[n]|$, then the pdf of $\mathcal{E}$ can be approximated by

$$f_{\mathcal{E}}(\epsilon) = \frac{1}{2\epsilon_{\max}}. \quad (54)$$

The corresponding estimation noise power is given by $\sigma_{\epsilon}^2 = (1/3)\epsilon_{\max}^2$. In order to show that $T_h^* = \epsilon_{\max}$, it suffices to compare the residual noise power in two cases

$$1)\ T_h > \epsilon_{\max}$$
$$2)\ T_h < \epsilon_{\max}.$$

Case 1)

When $T_h \geq \epsilon_{\max}$, a false alarm event does not occur [see (22)]. Therefore, (21) in Theorem 2 is simplified to

$$\sigma_{\gamma_r}^2(T_h) = P_{\text{der}}(T_h) \sigma_{\epsilon}^2 + P_{\text{uer}}(T_h) \sigma_{\text{uer}}^2(T_h) \quad (55)$$

where we explicitly indicate the dependency of $P_{\text{der}}, P_{\text{uer}}$, and σ_{uer} on T_h.

From (50), the probability of the UER event for given threshold T_h is

$$P_{\text{uer}}(T_h) = P_r(|Y_a - Y_e| \leq T_h, Y_a \neq y_o) = p_e \left(T_h - \frac{1}{4}\left(T_h^2 + \sigma_{\epsilon}^2\right) \right). \quad (56)$$

Note, since the DER and UER events are mutually exclusive, $P_{\text{der}} = p_e - P_{\text{uer}}$. From (56) and noting that $\epsilon_{\max} \leq T_h \ll 1$, we have

$$P_{\text{uer}}(T_h) > P_{\text{uer}}(\epsilon_{\max}) \quad (57)$$
$$P_{\text{der}}(T_h) < P_{\text{der}}(\epsilon_{\max}). \quad (58)$$

From (55), the difference between $\sigma_{\gamma_r}^2(T_h)$ and $\sigma_{\gamma_r}^2(\epsilon_{\max})$ is given by

$$\begin{aligned} &\sigma_{\gamma_r}^2(T_h) - \sigma_{\gamma_r}^2(\epsilon_{\max}) \\ &= (P_{\text{der}}(T_h) - P_{\text{der}}(\epsilon_{\max})) \sigma_{\epsilon}^2 \\ &\quad + \left(P_{\text{uer}}(T_h) \sigma_{\text{uer}}^2(T_h) - P_{\text{uer}}(\epsilon_{\max}) \sigma_{\text{uer}}^2(\epsilon_{\max}) \right) \\ &\geq (P_{\text{der}}(T_h) - P_{\text{der}}(\epsilon_{\max})) \sigma_{\epsilon}^2 \\ &\quad + (P_{\text{uer}}(T_h) - P_{\text{uer}}(\epsilon_{\max})) \sigma_{\text{uer}}^2(T_h) \end{aligned} \quad (59)$$

where we used the fact $\sigma_{\text{uer}}^2(T_h) > \sigma_{\text{uer}}^2(\epsilon_{\max})$. Given that $P_{\text{er}} = P_{\text{der}}(T_h) + P_{\text{uer}}(T_h) = P_{\text{der}}(\epsilon_{\max}) + P_{\text{uer}}(\epsilon_{\max})$ and $\sigma_{\text{uer}}^2 > \sigma_{\epsilon}^2$ [see (23)], we conclude

$$\sigma_{\gamma_r}^2(T_h) > \sigma_{\gamma_r}^2(\epsilon_{\max}). \quad (60)$$

Case 2)

When the threshold $T_h < \epsilon_{\max}$, P_{uer} decreases and P_{der} increases. However, in this case, false alarm probability P_{fer} increases, thereby degrading performance considerably. The difference of residual noise power $\Delta\sigma_{\gamma_r}^2 = \sigma_{\gamma_r}^2(T_h) - \sigma_{\gamma_r}^2(\epsilon_{\max})$ is given by

$$\begin{aligned} \Delta\sigma_{\gamma_r}^2 &= P_{\text{der}}(T_h) \sigma_{\epsilon}^2 + P_{\text{uer}}(T_h) \sigma_{\text{uer}}^2(T_h) \\ &\quad + P_{\text{fer}}(T_h) \sigma_{\text{uer}}^2(T_h) - P_{\text{der}}(\epsilon_{\max}) \sigma_{\epsilon}^2 \\ &\quad - P_{\text{uer}}(\epsilon_{\max}) \sigma_{\text{uer}}^2(\epsilon_{\max}). \end{aligned} \quad (61)$$

First, the difference in DER noise power term is

$$P_{\text{der}}(T_h) \sigma_{\epsilon}^2 - P_{\text{der}}(\epsilon_{\max}) \sigma_{\epsilon}^2 = \sigma_{\epsilon}^2 \Delta P \quad (62)$$

where ΔP is the increase in DER (decrease in UER) probability given by $\Delta P = P_{\text{der}}(T_h) - P_{\text{der}}(\epsilon_{\max}) = P_r(\epsilon_{\max} > |\gamma + \epsilon| > T_h)$. Similarly, from (23) and (24), UER noise power difference is given by

$$\begin{aligned} &P_{\text{uer}}(T_h) \sigma_{\text{uer}}^2(T_h) - P_{\text{uer}}(\epsilon_{\max}) \sigma_{\text{uer}}^2(\epsilon_{\max}) \\ &= p_e \left(\epsilon_{\max} - \frac{1}{4}\left(T_h^2 + \epsilon_{\max}^2\right) \right) \frac{\left(T_h^2 - \epsilon_{\max}^2\right)}{3} \\ &\quad - \left(\frac{\epsilon_{\max}^2}{3} + \sigma_{\epsilon}^2 \right) \Delta P. \end{aligned} \quad (63)$$

Finally, from (25), the FER noise power at T_h is

$$P_{\text{fer}}(T_h)\sigma^2_{\text{fer}}(T_h) = \frac{(1-p_e)}{3}\frac{(\epsilon_{\max}-T_h)\left(\epsilon^3_{\max}-T^3_h\right)}{\epsilon^2_{\max}}. \tag{64}$$

By hypothesis, ϵ is uniform in $[-\epsilon_{\max}, \epsilon_{\max}]$, we have following inequality

$$\begin{aligned}\Delta P &= P_r(\epsilon_{\max} > |\gamma+\epsilon| > T_h)\\ &\le P_r(\epsilon_{\max} > |\gamma| > T_h)\\ &= p_e\left(\left(T^2_h-\epsilon^2_{\max}\right)+4(\epsilon_{\max}-T_h)\right).\end{aligned} \tag{65}$$

With (62), (63), (64), (65), (61) can be rewritten as

$$\begin{aligned}\Delta\sigma^2_{\gamma_r} \ge{}& \frac{p_e}{3}\left(T_h-\frac{1}{4}\left(T^2_h+\sigma^2_\epsilon\right)\right)\left(T^2_h-\epsilon^2_{\max}\right)\\ &-\frac{p_e}{3}\left(\left(T^2_h-\epsilon^2_{\max}\right)+4(\epsilon_{\max}-T_h)\right)\epsilon^2_{\max}\\ &+\frac{(1-p_e)}{3}\frac{(\epsilon_{\max}-T_h)\left(\epsilon^3_{\max}-T^3_h\right)}{\epsilon^2_{\max}}.\end{aligned} \tag{66}$$

After some algebra, the right term in (66) is

$$\begin{aligned}&\frac{p_e}{3}\left(\left(T_h-\frac{1}{4}\left(T^2_h+\sigma^2_\epsilon\right)\right)\left(T^2_h-\epsilon^2_{\max}\right)-\left(\left(T^2_h-\epsilon^2_{\max}\right)\right.\right.\\ &\left.\left.+\ 4(\epsilon_{\max}-T_h)\right)\epsilon^2_{\max}+\frac{(\epsilon_{\max}-T_h)\left(\epsilon^3_{\max}-T^3_h\right)}{\epsilon^2_{\max}}\right)\\ &+\frac{1}{3}\frac{(\epsilon_{\max}-T_h)\left(\epsilon^3_{\max}-T^3_h\right)}{\epsilon^2_{\max}}.\end{aligned} \tag{67}$$

Since both first and second terms are positive (recalling $T_h < \epsilon_{\max} < 1$), $\Delta\sigma^2_{\gamma_r} \ge 0$.

From *Case 1)* and *Case 2)*, $T^*_h = \epsilon_{\max}$.

REFERENCES

[1] K. L. Shepard and V. Narayanan, "Noise in deep submicron digital design," in *Proc. IEEE/ACM Int. Conf. Comput.-Aided Des.*, 1996, pp. 524–531.

[2] J. R. Srour and J. M. McGarrity, "Radiation effects on microelectronics in space," *Proc. IEEE*, vol. 76, no. 11, pp. 1443–1469, Nov. 1988.

[3] V. De and S. Borkar, "Technology and design challenges for low power and high performance," in *Proc. Int. Symp. Low-Power Electron. Des.*, 1999, pp. 163–168.

[4] T. Karnik and S. Vangal, "Selective node engineering for chip-level soft error rate improvement," in *Proc. Symp. VLSI Circuits*, 2002, pp. 132–135.

[5] P. Hazucha and C. Svensson, "Impact of CMOS technology scaling on the atmospheric neutron soft error rate," *IEEE Trans. Nucl. Sci.*, vol. 47, no. 6, pp. 2586–2594, Dec. 2000.

[6] R. C. Baumann, "Soft errors in advanced semiconductor devices-Part I: The three radiation sources," *IEEE Trans. Device Mater. Reliab.*, vol. 1, no. 1, pp. 17–22, Mar. 2001.

[7] N. R. Shanbhag, K. Soumyanath, and S. Martin, "Reliable low-power design in the presence of deep submicron noise," in *Proc. Int. Symp. Low-Power Electron. Des.*, 2000, pp. 295–302.

[8] N. R. Shanbhag, "Reliable and efficient system-on-chip design," *IEEE Computer*, vol. 37, no. 3, pp. 42–50, Mar. 2004.

[9] Y. Tsiatouhas, T. Haniotakis, D. Nikolos, and C. Efstathiou, "Concurrent detection of soft errors based on current monitoring," in *On-Line Testing Workshop*, 2001, pp. 106–110.

[10] K. Zhang, S. Hareland, B. Senyk, and J. Maiz, "Methods for reducing soft errors in deep submicron integrated circuits," in *Proc. Solid-State Integr. Circuit Technol.*, 1998, pp. 516–519.

[11] J. M. Rabaey and M. Pedram, *Low Power Design Methodologies*. Norwell, MA: Kluwer, 1996, pp. 160–200.

[12] L. W. Massengill, A. E. Baranski, D. Nort, J. Meng, and B. L. Bhuva, "Analysis of single-event effects in combinational logic—Simulation of the AM2901 bitslice processor," *IEEE Trans. Nucl. Sci.*, vol. 47, no. 6, pp. 2609–2615, Dec. 2000.

[13] L. Wissel, S. Pheasant, R. Loughran, and C. LeBlanc, "Managing soft errors in ASICs," in *Proc. Custom Integr. Circuits Conf.*, 2002, pp. 85–88.

[14] P. Shivakumar, "Modeling the effect of technology trend on the soft error rate of combinational logic," in *Proc. Int. Conf. Dependable Syst. Netw.*, 2002, pp. 389–398.

[15] *"The 2003 International Technology Roadmap for Semiconductors,"* [Online]. Available: http://public.itrs.net.

[16] R. Baumann, "The impact of technology scaling on soft error rate performance and limits to the efficacy of error correction," in *Dig. Int. Electron Devices Meeting*, 2002, pp. 329–332.

[17] J. B. Nickel and A. K. Somani, "REESE: A method of soft error detection in microprocessors," *Dependable Syst. Netw.*, pp. 401–410, 2001.

[18] I. Yen, E. L. Leiss, and F. B. Bastani, "Exploiting redundancy to speed up parallel systems," in *Proc. Parallel Distributed Tech.*, 1993, pp. 51–60.

[19] L. Anghel, M. Nicolaidis, and M. Alzaher-Noufal, "Self-checking circuits versus realistic faults in very deep submicron," *Proc. IEEE VLSI Test Symp.*, pp. 55–63, 2000.

[20] L. Anghel, D. Alexandrescu, and M. Nicolaidis, "Evaluation of a soft error tolerance technique based on time and/or space redundancy," *Integr. Circuits Syst. Des.*, pp. 237–242, 2000.

[21] P. Mazumder, "An on-chip ECC for correcting soft errors in DRAM's with trench capacitors," *IEEE J. Solid-State Circuits.*, vol. 27, no. 11, pp. 1623–1633, Nov. 1992.

[22] T. Austin, "DIVA: A reliable substrate for deep submicron microarchitecture design," in *Proc. Int. Symp. Microarch.*, 1999, pp. 196–207.

[23] R. Hegde and N. R. Shanbhag, "Soft digital signal processing," *IEEE Trans. Very Large Scale Integr. (VLSI) Syst.*, vol. 9, no. 6, pp. 813–823, Dec. 2001.

[24] L. Wang and N. R. Shanbhag, "Low-power filtering via adaptive error-cancellation," *IEEE Trans. Signal Process.*, vol. 51, no. 2, pp. 575–583, Feb. 2003.

[25] B. Shim, S. Sridhara, and N. R. Shanbhag, "Low-Power digital signal processing via reduced precision redundancy," *IEEE Trans. Very Large Scale Integr. Syst.*, vol. 12, no. 5, pp. 497–510, May 2004.

[26] B. Shim, M. Zhang, and N. Shanbhag, "A novel forward-backward predictor based low-power DSP system," in *Proc. IEEE Workshop Signal Process. Syst. Implementation (SiPS)*, 2004, pp. 331–336.

[27] T. K. Moon and W. C. Striling, *Mathematical Methods and Algorithms for Signal Processing*. Englewood Cliffs, NJ: Prentice-Hall, 1999.

[28] K. G. Shin and H. Kim, "A time redundancy approach to TMR failures using fault-state likelihoods," *IEEE Trans. Computers*, vol. 43, no. 10, pp. 1151–1162, Oct. 1994.

[29] R. Hegde and N. R. Shanbhag, "A voltage overscaled low-power digital filter IC," *IEEE J. Solid-State Circuits*, vol. 39, no. 2, pp. 388–391, Feb. 2004.

[30] A. V. Oppenheim and R. Schafer, *Discrete-Time Signal Processing*. Englewood Cliffs, NJ: Prentice-Hall, 1989.

[31] A. Papoulis, *Probability, Random Variable, and Stochastic Processes*. New York: McGraw-Hill, 1991.

[32] M. Zhang and N. R. Shanbhag, "Soft error rate analysis (SERA)," in *Proc. IEEE/ACM Int. Conf. Comput.-Aided Des.*, 2004, pp. 111–118.

[33] T. Calin, "Upset hardened memory design for submicron CMOS technology," *IEEE Trans. Nucl. Sci.*, vol. 43, no. 6, pp. 2874–2878, Dec. 1996.

Byonghyo Shim (M'97) received the B.S. and M.S. degrees in control and instrumentation engineering from Seoul National University, Seoul, Korea, in 1995 and 1997, respectively, and the M.A. degree in mathematics and the Ph.D. degree in electrical and computer engineering from the University of Illinois at Urbana-Champaign, Urbana, in 2004 and 2005, respectively.

From 1997 to 2000, he was with the Department of Electronics Engineering at the Korean Air Force Academy as an Officer and an Academic Full-Time

Instructor. He had a short time research position in the DSP group of LG Electronics and DSP R&D Center, Texas Instruments Incorporated, Dallas, TX, in 1997 and 2004, respectively. In January 2005, he joined Qualcomm Inc., San Diego, CA, where he is currently a Senior Engineer working on wireless CDMA systems. His research interests encompass a wide spectrum of digital signal processing including signal processing for communication, VLSI signal processing, low-power and reliable signal processing, and estimation and detection and coding theory.

Dr. Shim was the recipient of the 2005 M. E. Van Valkenburg Research Award from the Electrical Computer Engineering Department of the University of Illinois and the 10th Samsung Humantech Paper Award in 2004. He is a member of Sigma Xi and Tau Beta Pi.

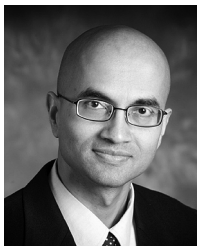

Naresh R. Shanbhag (F'06) received the Ph.D. degree in electrical engineering from the University of Minnesota, Minneapolis, in 1993.

From 1993 to 1995, he worked at AT&T Bell Laboratories, Murray Hill, NJ, where he was the lead chip architect for AT&T's 51.84-Mb/s transceiver chips over twisted-pair wiring for asynchronous transfer mode (ATM)-LAN and very high-speed digital subscriber line (VDSL) chip-sets. Since August 1995, he has been with the Department of Electrical and Computer Engineering and the Coordinated Science Laboratory, University of Illinois at Urbana-Champaign, Urbana, where he is currently a Professor. His research interests are in the design of integrated circuits and systems for broadband communications including low-power/high-performance VLSI architectures for error-control coding, equalization, as well as digital integrated circuit design. He has published more than 90 journal articles/book chapters/conference publications in this area and holds 3 U.S. patents. He is also a co-author of the research monograph *Pipelined Adaptive Digital Filters* (Kluwer, 1994).

Dr. Shanbhag was a recipient of the 2001 IEEE Transactions on VLSI Best Paper Award, the 1999 IEEE Leon K. Kirchmayer Best Paper Award, the 1999 Xerox Faculty Award, the National Science Foundation CAREER Award in 1996, and the 1994 Darlington Best Paper Award from the IEEE Circuits and Systems Society. From 1997–1999, he was a Distinguished Lecturer for the IEEE Circuits and Systems Society. From 1997–1999 and from 1999–2002, he served as an Associate Editor for the IEEE TRANSACTIONS ON CIRCUITS AND SYSTEMS: PART II and the IEEE TRANSACTIONS ON VERY LARGE SCALE INTEGRATION (VLSI) SYSTEMS, respectively. He has served on the technical program committees of various conferences.